A Model-Based Decomposition of the Sea Ice–Atmosphere Feedback over the Barents Sea during Winter

JESSICA LIPTAK AND COURTENAY STRONG

Department of Atmospheric Sciences, University of Utah, Salt Lake City, Utah

(Manuscript received 26 June 2013, in final form 21 October 2013)

ABSTRACT

The feedback between Barents Sea ice and the winter atmosphere was studied in a modeling framework by decomposing it into two sequential boundary forcing experiments. The Community Ice Code (CICE) model was initialized with anomalously high sea ice concentration (SIC) over the Barents Sea and forced with an atmosphere produced by positive SIC anomalies, and CICE was initialized with low Barents Sea SIC and forced with an atmosphere produced by negative SIC anomalies. Corresponding control runs were produced by exposing the same SIC initial conditions to climatological atmospheres, and the monthly mean sea ice response showed a positive feedback over the Barents Sea for both experiments: the atmosphere produced by positive SIC anomalies increased SIC over the Barents Sea during the winter, and the atmosphere produced by negative SIC anomalies decreased SIC. These positive feedbacks were driven primarily by thermodynamic forcing from surface longwave flux anomalies and were weakened somewhat by atmospheric temperature advection. Dynamical effects also opposed the positive feedback, with enhanced surface wind stress divergence over the Barents Sea in the high-SIC case and enhanced convergence in the low-SIC case.

1. Introduction

The interaction between Arctic sea ice and the atmosphere plays a large role in shaping local and hemispheric climate variability through changes in surface wind stress and turbulent heat fluxes. Physical reasoning suggests that negative sea ice anomalies locally induce upward sensible and latent heat flux anomalies, leading to decreased sea level pressure (SLP), cyclonic circulation, and surface convergence, while the opposite scenario occurs for positive sea ice anomalies. Sea ice, in turn, may respond to atmospheric variability associated with local flow regimes and large-scale teleconnection patterns.

On time scales shorter than one year, sea ice motion is primarily driven by surface wind stress (Thorndike and Colony 1982), where the direction of ice drift is approximately 30° to the right of the wind (Nansen 1902; Zubov 1943) and, as a general rule, parallel to surface isobars. Recent low September sea ice extent is associated with anticyclonic surface wind anomalies during the preceding summer (Ogi and Wallace 2007) that lead to enhanced poleward Ekman drift of the sea ice (Ogi et al. 2008). The recent decrease in summer sea ice over the western Arctic may also be attributed to anomalous anticyclonic flow, which is conducive to ice advection toward Fram Strait (Ogi and Rigor 2013). Low-level pressure and wind anomalies that enhance southward flow through Fram Strait are associated with increased sea ice export, and explain a large fraction of the variability in Arctic sea ice cover (Ogi et al. 2010). Fram Strait sea ice export is correlated with the second EOF of Arctic SLP, referred to as the dipole anomaly (Wu et al. 2006; Wang et al. 2009) and similar patterns (Tsukernik et al. 2010) that depict an east–west pressure gradient over Fram Strait. On a seasonal basis, the positive phase of the Arctic Oscillation (AO) is associated with enhanced ice export through Fram Strait and thinner ice over the eastern Arctic (Rigor et al. 2002; Zhang et al. 2003). Watanabe and Hasumi (2005) found that shifting the wind stress pattern from the negative phase of the AO to the positive phase increased Arctic sea ice export and decreased sea ice volume, while switching from the positive phase of the AO to the negative phase produced the opposite scenario. The positive phase of the North Atlantic Oscillation (NAO) (Hurrell et al. 2003) is also associated with enhanced Fram Strait

Corresponding author address: Courtenay Strong, University of Utah, 135 S, 1460 E, Rm. 819 (WBB), Salt Lake City, UT 84112-0110.
E-mail: court.strong@utah.edu

DOI: 10.1175/JCLI-D-13-00371.1

sea ice flux in winter (e.g., Kwok and Rothrock 1999; Kwok et al. 2004), although the correlation is only statistically significant after 1977 owing to the eastward shift in the NAO centers of action (Hilmer and Jung 2000).

The NAO also influences winter sea ice variability over the Labrador and Nordic Seas, where positive sea ice anomalies over the Labrador Sea and negative sea ice anomalies over the Greenland and Barents Seas are associated with the positive phase of the NAO (Deser et al. 2000; Vinje 2001). Several boundary forcing experiments with ice removal over the Barents Sea have also produced atmospheric patterns reminiscent of the NAO (Magnusdottir et al. 2004; Alexander et al. 2004 Seierstad and Bader 2009; Liptak and Strong 2014). Magnusdottir et al. showed that the feedback between North Atlantic ice cover and the NAO was negative; that is, the positive NAO reduces sea ice cover in the Barents Sea that, in turn, is conducive to the negative NAO. In addition, decomposition of the sea ice forcing revealed that the NAO-like response primarily resulted from sea ice concentration anomalies over the Barents Sea. The negative feedback was subsequently detected via statistical analysis of observations (Strong et al. 2009) and hybrid statistical–dynamical modeling (Strong and Magnusdottir 2010). In contrast, Ou (2013) proposed that the large-scale sea ice–atmosphere feedback over the Arctic was positive where, for example, negative SLP anomalies resulting from ice removal from the Barents Sea would strengthen the cyclonic circulation over the eastern Arctic, leading to further ice loss through Fram Strait.

Prior studies focused on the response of the atmosphere to monthly sea ice anomalies (Magnusdottir et al. 2004; Deser et al. 2004; Alexander et al. 2004; Koenigk et al. 2009; Seierstad and Bader 2009) or the effects of large-scale atmospheric forcing on sea ice on interannual and longer time scales (Koenigk et al. 2009; Zhang et al. 2010; Ogi et al. 2010). Here, we examine the feedback of the atmosphere onto sea ice over the Barents Sea, as it is the focal point of the large-scale sea ice–atmosphere feedback in the North Atlantic (Magnusdottir et al. 2004).

We focus on daily-to-monthly time scales during winter and decompose the feedback into two sequential boundary forcing experiments: an atmosphere model perturbed by imposed sea ice anomalies (Liptak and Strong 2014) and a sea ice–slab ocean model responding to the perturbed atmospheric fields. Although decomposition of the feedback into two sequential boundary forcing experiments may alter aspects of the interactions present in a coupled framework (e.g., Chen et al. 2013), this decomposition allows us to fully control the sea ice conditions that initiate the anomalous atmosphere–ocean exchanges. Specifically, we use atmospheric fields that developed in response to anomalously high and low sea ice, where the sea ice anomalies were restricted to the Barents Sea, were of uniform sign, and decayed realistically over the winter.

2. Data and methods

a. Model description

Version 4 of the stand-alone Community Atmosphere Model (CAM) (Neale et al. 2010) and Community Ice Code (CICE) model with a slab ocean (Hunke and Lipscomb 2008) were used to produce continuous control runs and winter experimental runs. The CAM and CICE are the atmosphere component and sea ice component of the Community Climate System Model/Community Earth System Model (CCSM/CESM) (Gent et al. 2011). The CAM has 26 vertical levels, and was run on a $1.9° \times 2.5°$ grid with a finite volume core (Lin 2004). CICE was run using five discrete ice thickness categories on a 1° displaced-pole grid with the pole centered over Greenland. We use gridbox-specific changes in sea ice concentration (SIC) due to thermodynamics (ΔTHM) and due to dynamics (ΔDYN) as diagnostics, and these fields are available as output from CICE. ΔTHM is computed by aggregating the changes in SIC (fraction/day) that result from fluxes of radiation, sensible, and latent heat. ΔDYN is the total change in SIC from wind and sea surface stress–induced ice deformation, transport, and ridging.

b. Experimental design

Table 1 summarizes nine simulations used in this study, and the associated notation, boundary conditions, and initial conditions for each are detailed in this section. Simulations denoted by I were CICE with a slab ocean and data atmosphere, and simulations denoted by A were CAM with data sea ice and sea surface temperatures (SSTs). The A_{100} is a continuous 100-yr control run forced with monthly climatological sea ice and SSTs from the merged Hadley Centre Sea Ice and SST (HadISST1) dataset and version 2 of the NOAA weekly optimum interpolation (OI) SST data (Hurrell et al. 2008). Output from A_{100} was used to produce a 100-yr continuous CICE control run (I_{100}).

To develop boundary conditions for the CAM experiments, climatological sea ice boundary conditions (BC_{CLIM}) were calculated from the long-term means of the daily winter (December–February) SIC in I_{100}. Then, an index of daily area-weighted SIC anomalies averaged over the region spanning 70°–82°N, 20°–65°E (black box in Fig. 1a) was calculated for each winter in I_{100}. The winter containing the most days with index

TABLE 1. The simulation name is given, along with the associated model and a summary of the boundary and initial conditions used.

Name	Model	Initial conditions	Boundary conditions	Role
A_{100}	CAM	Default	HadOIBl	Control
I_{100}	CICE	Default	A_{100}	Control
$A_{HIGH\text{-}SIC}$	CAM	1 Dec from each year of A_{100}	$BC_{HIGH\text{-}SIC}$	Expt
$A_{LOW\text{-}SIC}$	CAM	1 Dec from each year of A_{100}	$BC_{LOW\text{-}SIC}$	Expt
A_{CLIM}	CAM	1 Dec from each year of A_{100}	BC_{CLIM}	Control
$I_{HIGH\text{-}SIC}$	CICE	1 Dec from each year of $BC_{HIGH\text{-}SIC}$	$A_{HIGH\text{-}SIC}$	Expt
$I_{CLIM\text{-}H}$	CICE	1 Dec from each year of $BC_{HIGH\text{-}SIC}$	A_{CLIM}	Control
$I_{LOW\text{-}SIC}$	CICE	1 Dec from each year of $BC_{LOW\text{-}SIC}$	$A_{LOW\text{-}SIC}$	Expt
$I_{CLIM\text{-}L}$	CICE	1 Dec from each year of $BC_{LOW\text{-}SIC}$	A_{CLIM}	Control

values more than one standard deviation (1σ) above the I_{100} long-term winter mean was identified (55 days $> 1\sigma$), and the SIC from each winter day of the anomalous year was subtracted from corresponding daily values of the long-term winter mean to create anomalies. The SIC anomalies over the Barents Sea were superimposed onto BC_{CLIM}, yielding high-SIC boundary conditions ($BC_{HIGH\text{-}SIC}$); low-SIC boundary conditions ($BC_{LOW\text{-}SIC}$) were prepared analogously from the winter containing the most days with index values more than 1σ below the I_{100} long-term winter mean (50 days $< -1\sigma$). The experiments $A_{HIGH\text{-}SIC}$ and $A_{LOW\text{-}SIC}$ were forced by $BC_{HIGH\text{-}SIC}$ and $BC_{LOW\text{-}SIC}$, respectively. The control run (A_{CLIM}) was forced with BC_{CLIM} so that the daily sea ice boundary forcing was identical at all grid points in $A_{HIGH\text{-}SIC}$, $A_{LOW\text{-}SIC}$, and A_{CLIM} except over the Barents Sea. Figure 1 shows the monthly mean values of the daily SIC anomalies for the $A_{HIGH\text{-}SIC}$ and $A_{LOW\text{-}SIC}$ experiments. The $A_{HIGH\text{-}SIC}$, $A_{LOW\text{-}SIC}$, and A_{CLIM} sea ice boundary conditions were regridded to the $1.9° \times 2.5°$ CAM grid, and CAM was run for 100 winters initialized with 1 December conditions taken from each year of A_{100}. In section 3, we present atmospheric anomalies from $A_{HIGH\text{-}SIC}$ and $A_{LOW\text{-}SIC}$ that are of direct relevance to the sea ice responses investigated in this study, and additional details on larger-scale patterns in these atmospheric experiments are given in Liptak and Strong (2014).

To investigate how $A_{HIGH\text{-}SIC}$ feeds back onto the sea ice, we forced CICE with $A_{HIGH\text{-}SIC}$ using 1 December fields from $BC_{HIGH\text{-}SIC}$ as initial conditions for the experiment $I_{HIGH\text{-}SIC}$. The associated control run was the same, but forced by A_{CLIM}, and is denoted $I_{CLIM\text{-}H}$. Likewise, the feedback of $A_{LOW\text{-}SIC}$ onto the sea ice was studied by forcing CICE with $A_{LOW\text{-}SIC}$ for the experiment $I_{LOW\text{-}SIC}$, and with A_{CLIM} for the corresponding control run $I_{CLIM\text{-}L}$ using 1 December fields from $BC_{LOW\text{-}SIC}$ as initial conditions.

The CAM and CICE experiments were each run for 100 winters, and their output was averaged over their respective ensemble members to form daily means. The responses of the CAM runs were defined as the anomalies produced by subtracting the ensemble mean A_{CLIM} atmospheric fields for each day of winter: $A_{HIGH\text{-}SIC} - A_{CLIM}$ and $A_{LOW\text{-}SIC} - A_{CLIM}$. For the CICE runs, the responses were analogously defined as $I_{HIGH\text{-}SIC} - I_{CLIM\text{-}H}$ and $I_{LOW\text{-}SIC} - I_{CLIM\text{-}L}$. $I_{HIGH\text{-}SIC} - I_{CLIM\text{-}H}$ is referred to as the high-SIC response, and $I_{LOW\text{-}SIC} - I_{CLIM\text{-}L}$ is referred to as the low-SIC response in the remaining text. Daily response values were averaged to monthly values for most of the presented results, and statistical significance of the responses was determined at the 95% confidence level by bootstrapping the distributions of each response 1000 times (e.g., Efron 1979).

3. Results

a. *Response of high-SIC initial conditions to the high-SIC atmosphere*

Figures 2a–c show the monthly mean responses of the sea ice concentration over the Barents Sea for high-SIC initial conditions and boundary forcing by $A_{HIGH\text{-}SIC}$. In all three months, the sign of the SIC response is positive, indicating a positive sea ice–atmosphere feedback over the Barents Sea; that is, for the same high-SIC initial conditions, $A_{HIGH\text{-}SIC}$ atmospheric conditions produce more sea ice over the Barents Sea than A_{CLIM} conditions. The magnitudes and extents of the SIC responses follow the evolution of the SIC anomalies used to force $A_{HIGH\text{-}SIC}$ (Figs. 1a–c), decreasing from December to February. Statistically significant SIC responses are confined to the Barents Sea in all months except February, when small positive and negative responses are present over the Bering Sea (not shown), indicating that the positive sea ice–atmosphere feedback is a local feature despite the presence of NAO-like large-scale circulation differences in the boundary forcing atmospheres of the experiment and the control (Liptak and Strong 2014).

In December, the response of the rate of change in SIC due to thermodynamics (ΔTHM, Fig. 3a) is positive over most of the corresponding SIC response (Fig. 2a),

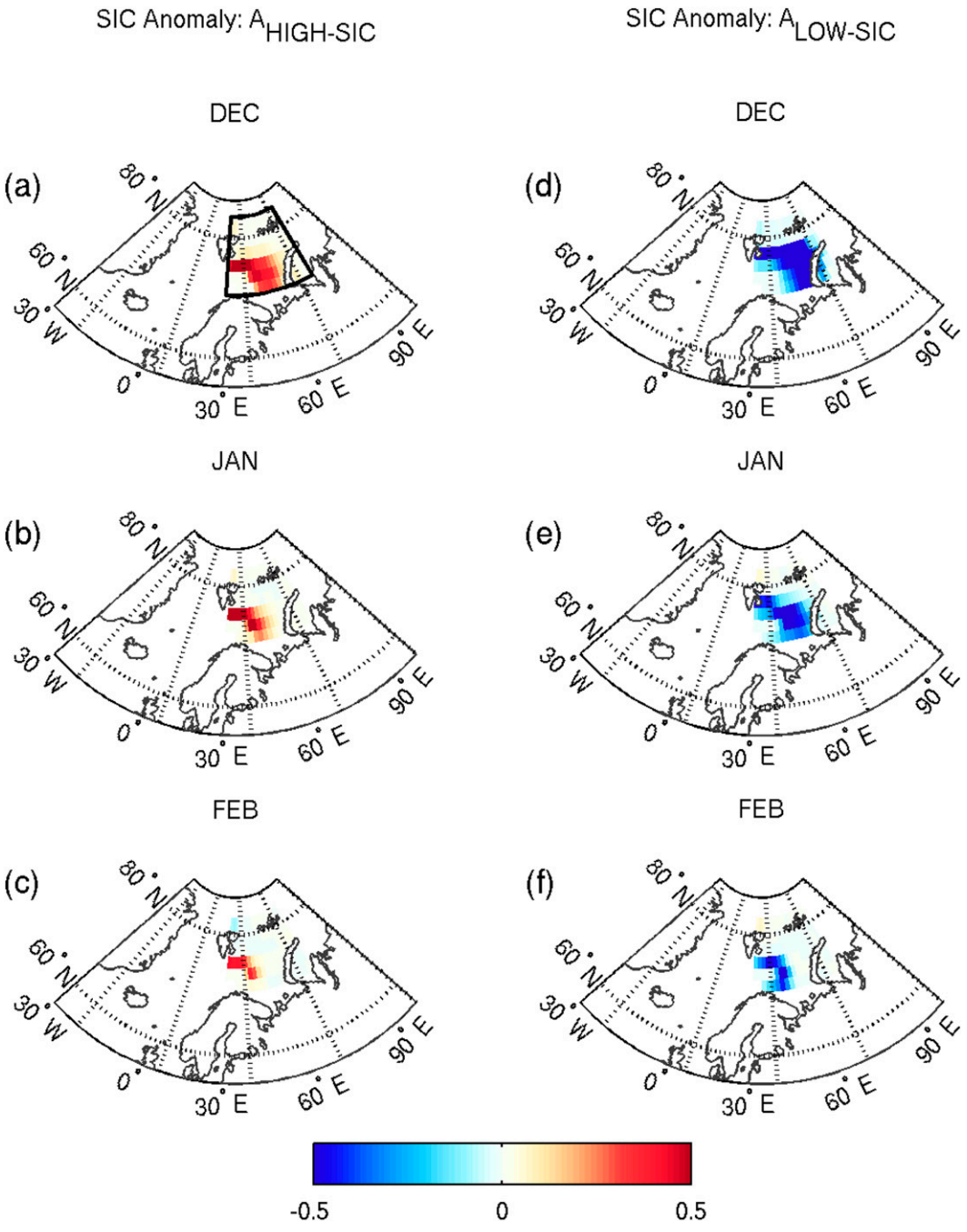

FIG. 1. Monthly means (December–February) of the daily SIC anomalies (fraction) used to force CAM in the (a)–(c) high-SIC and (d)–(f) low-SIC experiments. The black box in (a) outlines the area used to define the Barents Sea.

indicating that thermodynamic processes contribute to the positive feedback except over the western Barents Sea where the ΔTHM response is negative. In contrast, the subsequent ΔTHM response patterns (Figs. 3b,c) are weaker, being positive over the center of the SIC response region, and negative elsewhere. As detailed later in this subsection, these ΔTHM effects stem principally from downwelling longwave forcing associated with anomalously low air temperatures in the $A_{HIGH\text{-}SIC}$ boundary conditions. Figures 3d–f (shading) shows that the responses of the rate of change in SIC from dynamics (ΔDYN) are similar for each month, with negative anomalies over the center of the SIC response region where the wind stress response is divergent (arrows, Figs. 3d–f), and

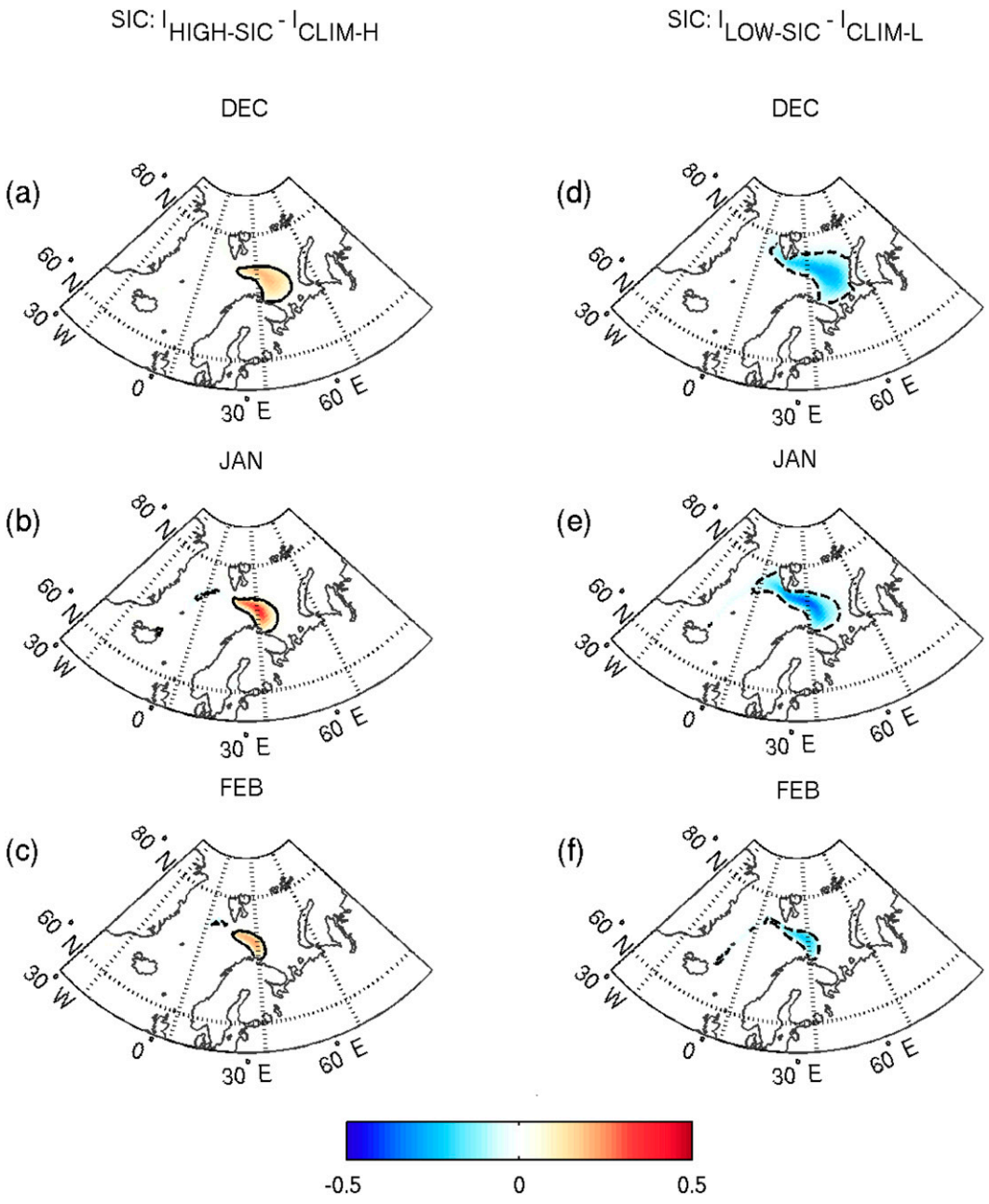

FIG. 2. Monthly mean responses of SIC (fraction) over the Barents Sea for the (a)–(c) high-SIC and (d)–(f) low-SIC CICE experiments. Values that are statistically significant at the 95% confidence level are shaded. Solid (dashed) curves indicate the 0.05 (−0.05) contours.

positive anomalies over the western edge where the wind stress response is convergent.

Illustrating the temporal evolution of the response, Fig. 4a shows that daily mean Barents Sea SIC is greater in $I_{HIGH\text{-}SIC}$ than $I_{CLIM\text{-}H}$ for most of the winter, with both values converging in February as the SIC anomaly used to force $A_{HIGH\text{-}SIC}$ weakens (Figs. 1a–c) and the ice cover increases. As a result, the daily mean SIC response over the Barents Sea (Fig. 4b) maximizes in mid-December, then steadily declines in January and February, remaining positive throughout the winter. The daily ΔTHM response (Fig. 4c) starts out positive, peaks in December, then oscillates around zero for the remainder of winter. The daily ΔDYN response (Fig. 4c) is weaker and predominantly negative. Thus, the daily and monthly mean ΔTHM and ΔDYN responses indicate

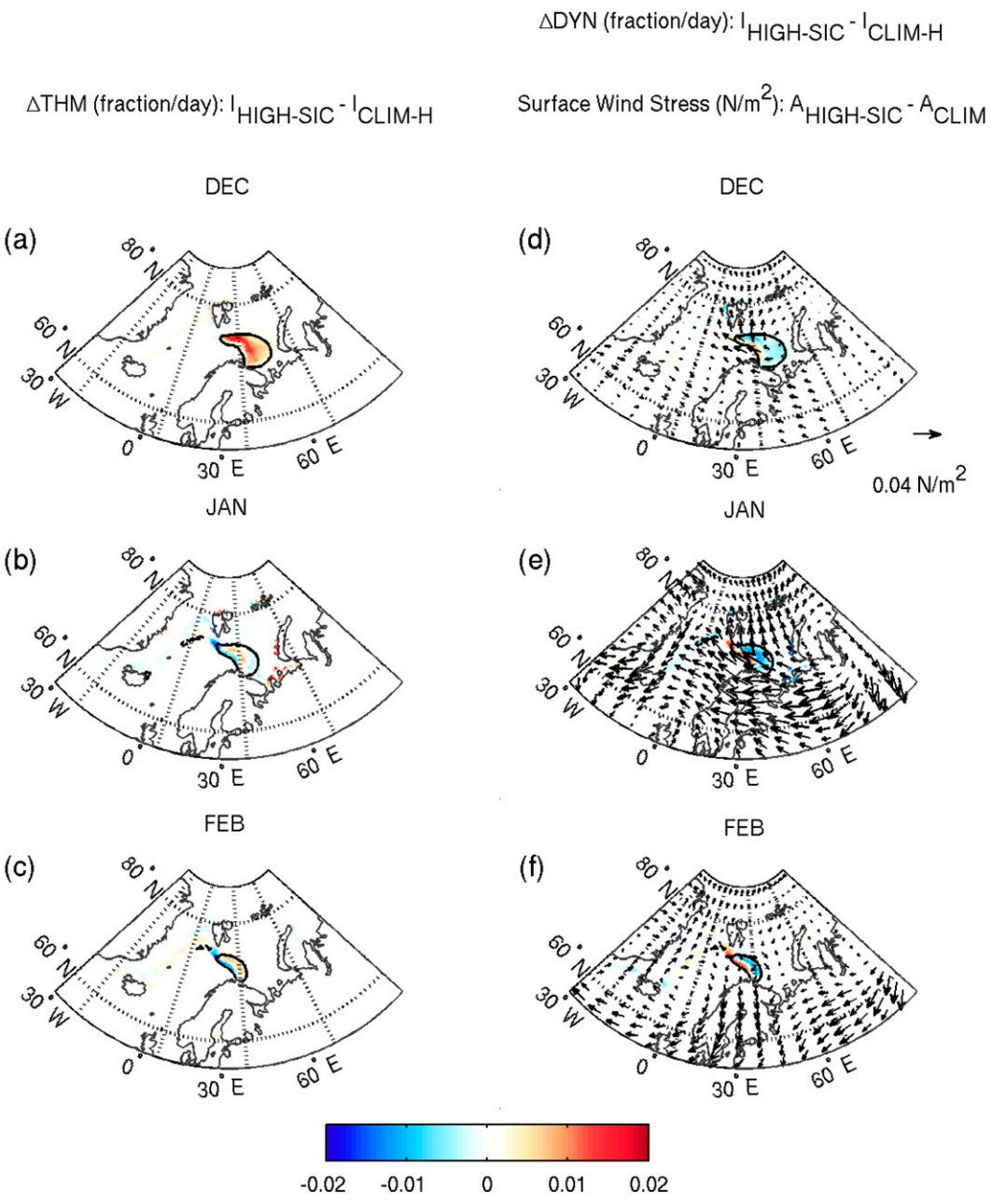

FIG. 3. For the high-SIC experiments: (a)–(c) monthly mean responses of the change in SIC due to thermodynamics and (d)–(f) the change in SIC due to dynamics (shading). Units are fraction day^{-1}. Arrows show the wind stress anomaly (N m^{-2}) for $A_{HIGH\text{-}SIC} - A_{CLIM}$. Black solid and dashed curves are copied from Fig. 2. Values are shaded where the ΔTHM responses in (a)–(c) and ΔDYN responses in (d)–(f) are statistically significant at the 95% confidence level.

that the positive SIC response over the Barents Sea is thermodynamically driven, and that dynamical processes (i.e., deformation and transport) tend to oppose the feedback.

Monthly mean differences in the atmospheric boundary conditions provided by $A_{HIGH\text{-}SIC}$ and A_{CLIM} show that negative downwelling surface longwave radiation anomalies (Figs. 5a–c) align with positive ΔTHM anomalies (Figs. 3a–c) over the centers of the corresponding positive SIC responses. The responses in temperature advection, calculated by applying $-\mathbf{V} \cdot \nabla T$ to the lowest model level temperature and wind components, show opposite-signed anomalies over the eastern and western sides of the ice anomaly region (Figs. 5d–f). These dipole

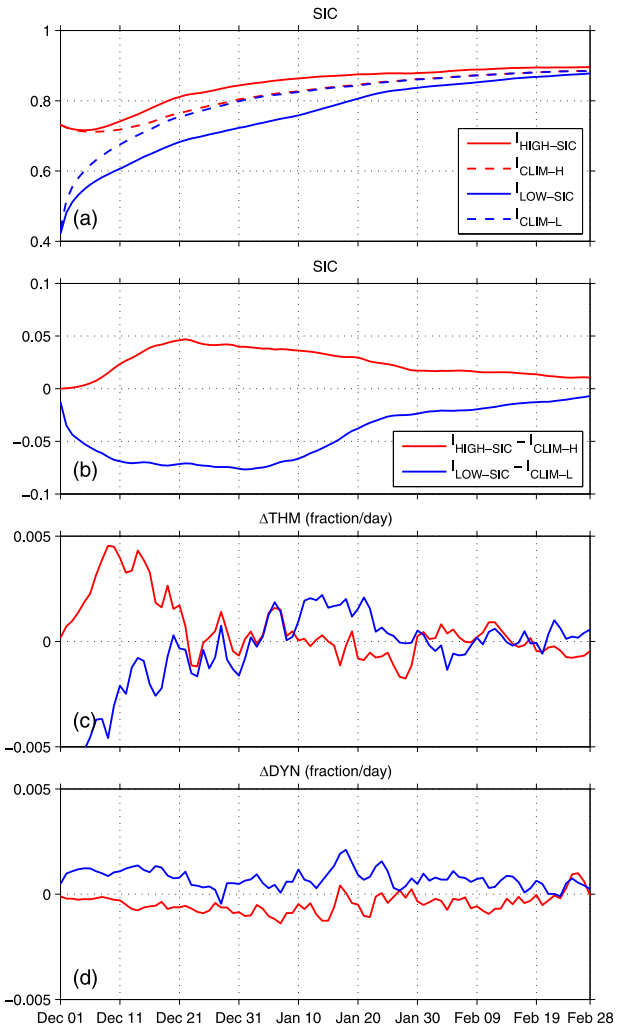

FIG. 4. (a) Daily mean SIC (fraction) over the Barents Sea for the high-SIC experiment (solid red line) and control run (dashed red line), and the low-SIC experiment (solid blue line) and control run (dashed blue line). Responses of the daily means in (b) SIC (fraction), (c) the change in SIC due to thermodynamics, and (d) the change in SIC due to dynamics for the high-SIC (solid red lines) and low-SIC (solid blue lines) conditions. The blue curve in (c) begins off the scale at −0.03 on 1 Dec.

patterns match the expected response, given a packet of anomalously cold air over the added sea ice, and act to somewhat weaken the cold anomaly. More specifically, positive temperature advection anomalies in the high-SIC atmosphere over the eastern SIC response region are consistent with large-scale flow from the relatively warm continent over positive SIC anomalies shown in Figs. 1a–c, and negative temperature advection anomalies near the western edge of the SIC response region result from flow over the positive SIC anomalies toward the exposed ocean. The surface shortwave radiation response (not shown) is small and is limited to the end of February when polar night ends over the southern half of the Barents Sea.

The alignment of the negative downwelling longwave radiation anomalies with the SIC responses and negative low-level temperature anomalies (not shown) throughout the winter indicates that surface longwave forcing drives the positive sea ice–atmosphere feedback by providing a persistent source of anomalously cold air over the Barents Sea. Effects more directly related to wind, including wind stress divergence and temperature advection, only partially offset the longwave radiative-driven increase in ice.

b. *Response of low-SIC initial conditions to the low-SIC atmosphere*

The monthly mean SIC responses for the low-SIC experiment (Figs. 2d–f) show a localized positive sea ice–atmosphere feedback over the Barents Sea throughout the winter, with statistically significant SIC responses limited to the Barents Sea until February when smaller negative SIC anomalies are also present in the Labrador Sea and Sea of Okhotsk (not shown). The monthly ΔTHM (Figs. 6a–c) and ΔDYN (Figs. 6d–f) responses depict patterns that are analogous to the corresponding high-SIC responses but opposite in sign and indicate that thermodynamic processes outweigh dynamics to reduce SIC over the Barents Sea in the low-SIC response.

Temporally, daily mean Barents Sea SIC (Fig. 4a) increases in $I_{LOW\text{-}SIC}$ and $I_{CLIM\text{-}L}$ throughout the winter, converging in February as the SIC anomaly used to force $A_{LOW\text{-}SIC}$ weakens (Figs. 1d–f), and producing a negative daily SIC response that peaks in December (Fig. 4b). The strong negative ΔTHM response in December (Fig. 4c) outweighs the positive response in January and the weak positive ΔDYN response (Fig. 4d), resulting in the negative monthly mean SIC responses shown in Figs. 2d–f. Initially, the thermodynamic forcing is stronger in the low-SIC experiment than in the high-SIC experiment (Fig. 4c), reflecting the differences in the strength of the SIC anomalies used to force $A_{LOW\text{-}SIC}$ and $A_{HIGH\text{-}SIC}$ (Fig. 1). As a result, the SIC response in the low-SIC experiment becomes negative a few hours following initialization (not shown), producing a negative daily average 1 December SIC response (Fig. 4b), whereas the high-SIC response visibly differs from zero after approximately 2 days.

The difference in atmospheric boundary conditions ($A_{LOW\text{-}SIC} - A_{CLIM}$) shows positive downwelling longwave radiation anomalies over the SIC response region (Figs. 7a–c) that result from increased longwave radiation at the surface in $A_{LOW\text{-}SIC}$. As in the high-SIC experiment, positive low-level temperature anomalies (not shown) that are collocated with the positive SIC

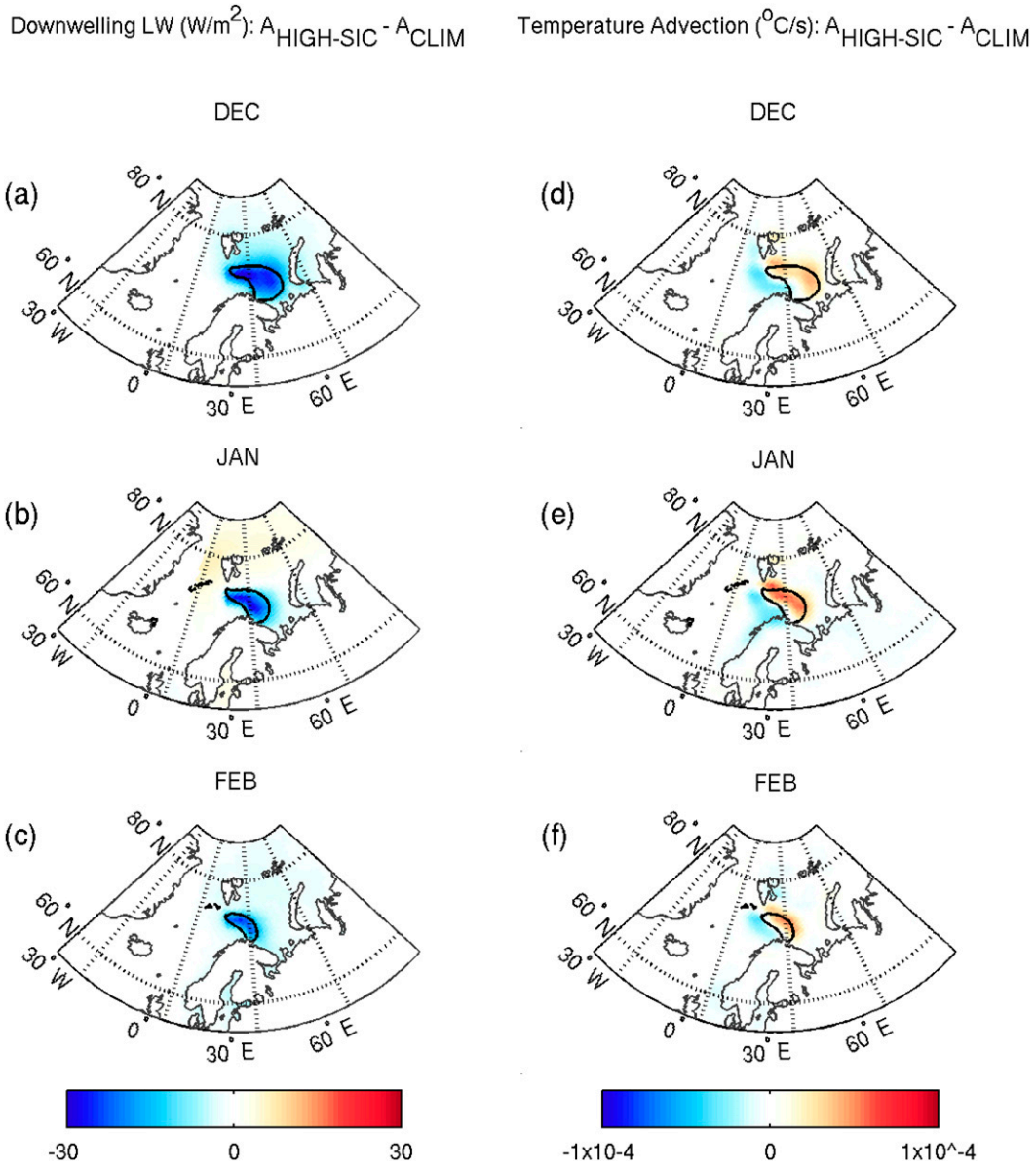

FIG. 5. Difference in atmospheric boundary conditions calculated as $A_{HIGH\text{-}SIC} - A_{CLIM}$: (a)–(c) downwelling longwave radiation flux at the surface (W m^{-2}) and (d)–(f) temperature advection (°C s^{-1}) at the lowest model level: black solid and dashed curves copied from Fig. 2. The responses have been linearly interpolated from the regular CAM grid to the displaced pole CICE grid for display only.

responses indicate that longwave forcing produces anomalously warm air that drives the positive sea ice–atmosphere feedback. Dipole patterns in the temperature advection response (Figs. 7d–f) are again consistent with, and somewhat weaken, the positive temperature anomalies over the area where ice cover is reduced. Negative temperature advection anomalies over the eastern SIC response region result from increased cold advection in $A_{LOW\text{-}SIC}$ as offshore flow moves over the negative SIC anomalies. Surface wind stress convergence (arrows, Figs. 6d–f) aligns with the positive ΔDYN response (shading, Figs. 6d–f) and opposes the positive sea ice–atmosphere feedback over the center of the SIC response, while divergence supports the feedback over the western edge where the ΔDYN response is negative.

4. Discussion and conclusions

The winter responses of Barents Sea ice to atmospheric boundary conditions generated by daily positive

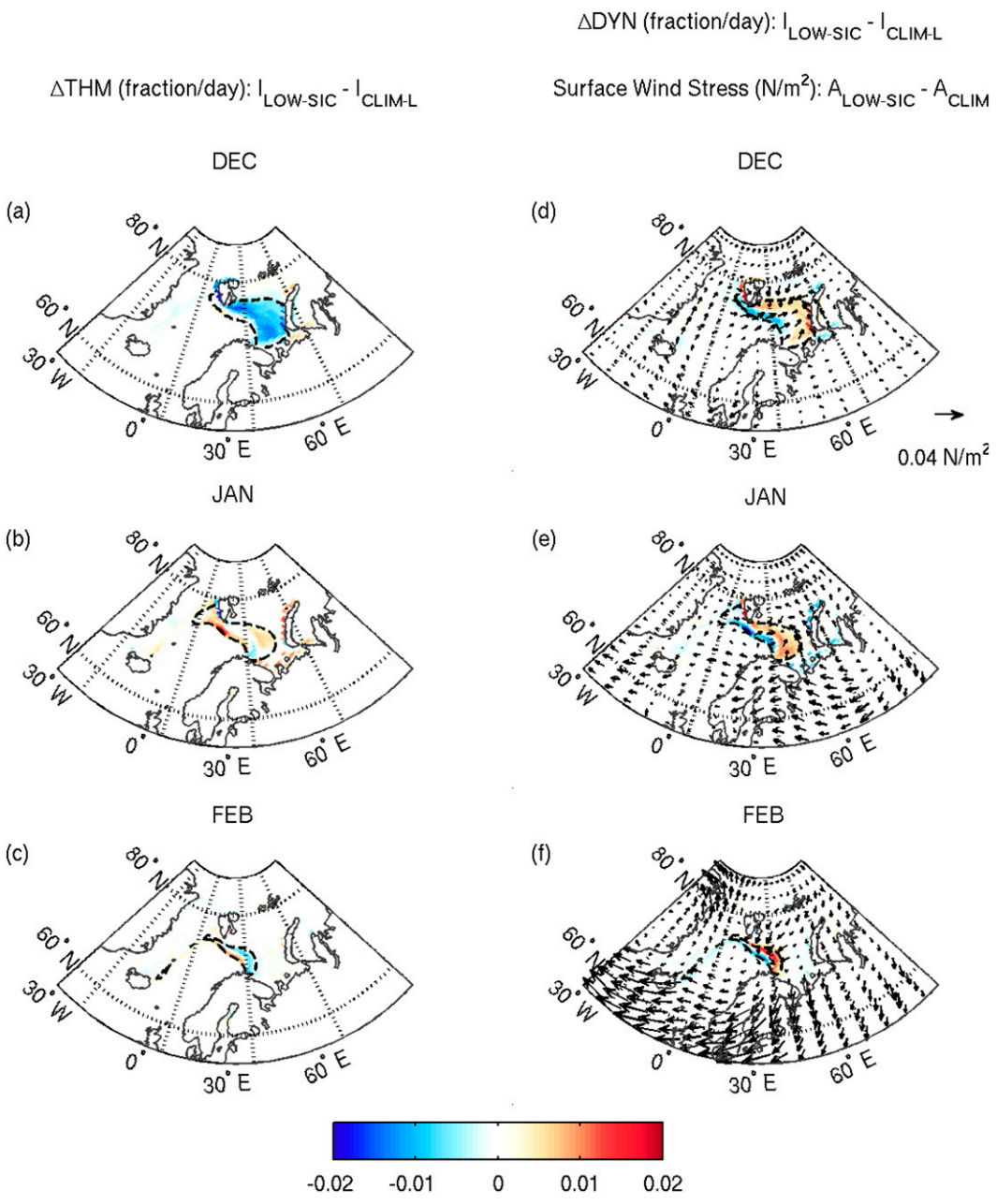

FIG. 6. As in Fig. 3, but for the low-SIC experiment.

and negative SIC anomalies indicate a sea ice–atmosphere feedback that is local and positive despite the presence of large-scale NAO-like changes in the atmospheric circulation. The positive feedback was thermodynamically driven, where negative surface downwelling longwave radiation anomalies increased SIC in the high-SIC experiment, and positive downwelling longwave radiation anomalies decreased SIC in the low-SIC experiment. In both experiments, temperature advection opposed the positive feedback by weakening ice-induced air temperature anomalies. Dynamical forcing countered the positive feedback owing to surface wind stress divergence over the Barents Sea in the high-SIC experiment, and wind stress convergence in the low-SIC experiment. The magnitude of the positive feedback peaked in December and decreased during the remaining winter months as the strength of the atmospheric forcing declined and the ice filled in.

Our results contrast the large-scale NAO-driven negative sea ice–atmosphere feedback over the Barents Sea

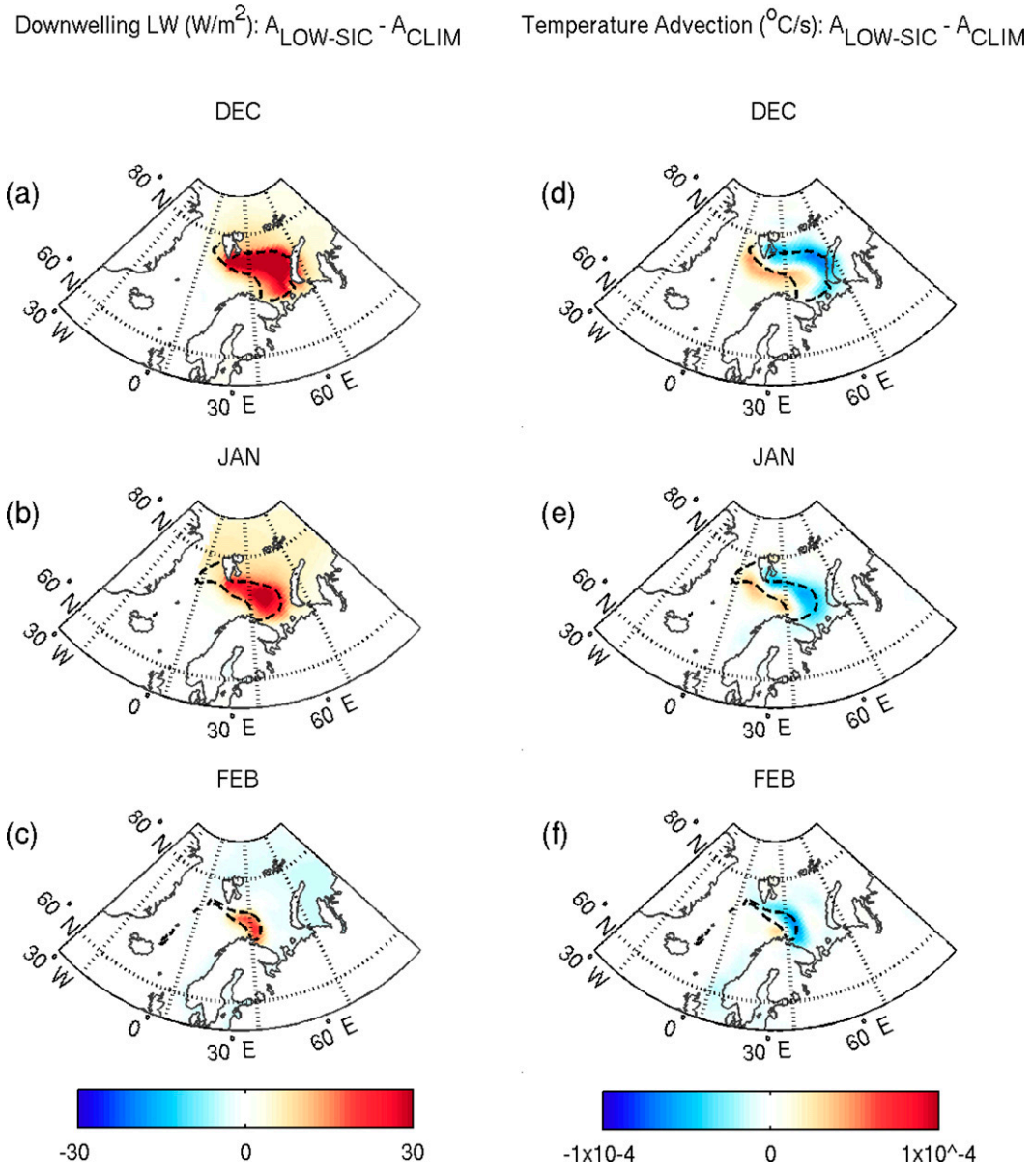

FIG. 7. As in Fig. 5, but for the low-SIC experiment.

implied by and investigated in prior work (Magnusdottir et al. 2004; Strong et al. 2009; Strong and Magnusdottir 2010) and highlight how local processes may influence the sign of the overall feedback. Importantly, results here are based on decomposing the feedback into sequential boundary forcing experiments using stand-alone sea ice and atmosphere components. The uncoupled atmosphere provided sources of sustained anomalously cold and warm air over the Barents Sea so that the thermodynamic forcing from downwelling longwave flux anomalies outweighed advection and dynamic forcing and determined the net sea ice responses. Had the sea ice been coupled to the atmosphere, dynamic forcing would have likely played a larger role in determining the sign and magnitude of the feedback, as demonstrated by Koenigk et al. (2009), who found that ice transport between the Barents Sea and central Arctic was the main driver of the interannual variability of sea ice volume over the Barents Sea in coupled sea ice–ocean–atmosphere model. Using May–September 1990 boundary conditions, Maslanik et al. (2000) showed that sea ice loss in the eastern Arctic in a stand-alone dynamic–thermodynamic ice model primarily resulted from melting, while both melting and ice divergence contributed to sea ice loss in

a coupled sea ice–atmosphere–slab ocean model. Local differences in the variance of the atmospheric responses in coupled and uncoupled models forced with identical boundary conditions are related to variations in the interference of SST-forced responses with weather-related ''noise'' (Chen et al. 2013), and Bretherton and Battisti (2000) provide additional insights into the dynamics and interpretation of boundary-forcing experiments. Work is under way to further examine the sea ice–atmosphere feedback by allowing and suppressing it in a coupled modeling framework.

Acknowledgments. This research was supported by the National Science Foundation Arctic Sciences Division Grant 1022485. Provision of computer infrastructure by the Center for High Performance Computing at the University of Utah is gratefully acknowledged.

REFERENCES

Alexander, M. A., U. S. Bhatt, J. E. Walsh, M. S. Timlin, J. S. Miller, and J. D. Scott, 2004: The atmospheric response to realistic Arctic sea ice anomalies in an AGCM during winter. *J. Climate,* **17,** 890–905, doi:10.1175/1520-0442(2004)017<0890:TARTRA>2.0.CO;2.

Bretherton, C. S., and D. S. Battisti, 2000: An interpretation of the results from atmospheric general circulation models forced by the time history of the observed sea surface temperature distribution. *Geophys. Res. Lett.,* **27** (6), 767–770, doi:10.1029/1999GL010910.

Chen, H., E. K. Shneider, B. P. Kirtman, and I. Colfescu, 2013: Evaluation of weather noise and its role in climate model simulations. *J. Climate,* **26,** 3766–3784, doi:10.1175/JCLI-D-12-00292.1.

Deser, C., J. E. Walsh, and M. S. Timlin, 2000: Arctic sea ice variability in the context of recent atmospheric circulation trends. *J. Climate,* **13,** 617–633, doi:10.1175/1520-0442(2000)013<0617:ASIVIT>2.0.CO;2.

——, G. Magnusdottir, R. Saravanan, and A. S. Phillips, 2004: The effects of North Atlantic SST and sea-ice anomalies on the winter circulation in CCM3. Part II: Direct and indirect components of the response. *J. Climate,* **17,** 877–889, doi:10.1175/1520-0442(2004)017<0877:TEONAS>2.0.CO;2.

Efron, B., 1979: Bootstrap methods: Another look at the jackknife. *Ann. Stat.,* **7,** 1–26, doi:10.1214/aos/1176344552.

Gent, P. R., and Coauthors, 2011: The Community Climate System Model version 4. *J. Climate,* **24,** 4973–4991, doi:10.1175/2011JCLI4083.1.

Hilmer, M., and T. Jung, 2000: Evidence for a recent change in the link between the North Atlantic Oscillation and Arctic sea ice export. *Geophys. Res. Lett.,* **27** (7), 989–992, doi:10.1029/1999GL010944.

Hunke, E. C., and W. H. Lipscomb, 2008: CICE: The Los Alamos sea ice model user's manual, version 4. Tech. Rep. LA-CC-06-012, Los Alamos National Laboratory, 76 pp.

Hurrell, J. W., Y. Kushnir, G. Ottersen, and M. Visbeck, 2003: *The North Atlantic Oscillation: Climate Significance and Environmental Impact. Geophys. Monogr.,* Vol. 134, Amer. Geophys. Union, 279 pp.

——, J. J. Hack, D. Shea, J. M. Caron, and J. Rosinski, 2008: A new sea surface temperature and sea ice boundary dataset for the Community Atmosphere Model. *J. Climate,* **21,** 5145–5153, doi:10.1175/2008JCLI2292.1.

Koenigk, T., U. Mikolajewicz, J. H. Jungclaus, and A. Kroll, 2009: Sea ice in the Barents Sea: Seasonal to interannual variability and climate feedbacks in a global coupled model. *Climate Dyn.,* **32,** 1119–1138, doi:10.1007/s00382-008-0450-2.

Kwok, R., and D. A. Rothrock, 1999: Variability of Fram Strait ice flux and North Atlantic Oscillation. *J. Geophys. Res.,* **104,** 5177–5189, doi:10.1029/1998JC900103.

——, G. F. Cunningham, and S. S. Pang, 2004: Fram Strait sea ice outflow. *J. Geophys. Res.* **109,** C01009, doi:10.1029/2003JC001785.

Lin, S.-J., 2004: A ''vertically Lagrangian'' finite-volume dynamical core for global models. *Mon. Wea. Rev.,* **132,** 2293–2307, doi:10.1175/1520-0493(2004)132<2293:AVLFDC>2.0.CO;2.

Liptak, J., and C. Strong, 2014: The winter atmospheric response to sea ice anomalies in the Barents Sea. *J. Climate,* **27,** 914–924, doi:10.1175/JCLI-D-13-00186.1.

Magnusdottir, G., C. Deser, and R. Saravanan, 2004: The effects of North Atlantic SST and sea ice anomalies on the winter circulation in CCM3. Part I: Main features and storm track characteristics of the response. *J. Climate,* **17,** 857–876, doi:10.1175/1520-0442(2004)017<0857:TEONAS>2.0.CO;2.

Maslanik, J. A., A. H. Lynch, M. C. Serreze, and W. Wu, 2000: A case study of regional climate anomalies in the Arctic: Performance requirements for a coupled model. *J. Climate,* **13,** 383–401, doi:10.1175/1520-0442(2000)013<0383:ACSORC>2.0.CO;2.

Nansen, F., 1902: *The Oceanography of the North Polar Basin.* Longmans, Green, and Company, 427 pp.

Neale, R. B., and Coauthors, 2010: Description of the NCAR Community Atmosphere Model (CAM 4.0). NCAR Tech. Note NCAR/TN-485+STR, 212 pp. [Available online at http://www.cesm.ucar.edu/models/ccsm4.0/cam/docs/description/cam4_desc.pdf.]

Ogi, M., and J. M. Wallace, 2007: Summer minimum Arctic sea ice extent and the associated summer atmospheric circulation. *Geophys. Res. Lett.,* **34,** L12705, doi:10.1029/2007GL029897.

——, and I. G. Rigor, 2013: Trends in Arctic sea ice and the role of atmospheric circulation. *Atmos. Sci. Lett.,* **14** (2), 97–101, doi:10.1002/asl2.423.

——, ——, M. G. McPhee, and J. M. Wallace, 2008: Summer retreat of Arctic sea ice: Role of summer winds. *Geophys. Res. Lett.,* **35,** L24701, doi:10.1029/2008GL035672.

——, K. Yamazaki, and J. M. Wallace, 2010: Influence of winter and summer surface wind anomalies on summer Arctic sea ice extent. *Geophys. Res. Lett.,* **37,** L07701, doi:10.1029/2009GL042356.

Ou, H.-W., 2013: A box model of the Arctic natural variability. *Climate Dyn.,* **40** (7–8), 1687–1706, doi:10.1007/s00382-012-1453-6.

Rigor, I. G., J. M. Wallace, and R. L. Colony, 2002: Response of sea ice to the Arctic Oscillation. *J. Climate,* **15,** 2648–2663, doi:10.1175/1520-0442(2002)015<2648:ROSITT>2.0.CO;2.

Seierstad, I., and J. Bader, 2009: Impact of a projected future Arctic sea ice reduction on extratropical storminess and the NAO. *Climate Dyn.,* **33** (7), 937–943, doi:10.1007/s00382-008-0463-x.

Strong, C., and G. Magnusdottir, 2010: Dependence of NAO variability on coupling with sea ice. *Climate Dyn.,* **36** (9–10), 1681–1689, doi:10.1007/s00382-010-0752-z.

——, ——, and H. Stern, 2009: Observed feedback between winter sea ice and the North Atlantic Oscillation. *J. Climate,* **22,** 6021–6032, doi:10.1175/2009JCLI3100.1.

Thorndike, A. S., and R. Colony, 1982: Sea ice motion in response to geostrophic winds. *J. Geophys. Res.,* **87** (C8), 5845–5852, doi:10.1029/JC087iC08p05845.

Tsukernik, M., C. Deser, M. Alexander, and R. Tomas, 2010: Atmospheric forcing of Fram Strait sea ice export: A closer look. *Climate Dyn.,* **35,** 1349–1360, doi:10.1007/s00382-009-0647-z.

Vinje, T., 2001: Anomalies and trends in sea-ice extent and atmospheric circulation in the Nordic Seas during the period 1864–1998. *J. Climate,* **14,** 255–267, doi:10.1175/1520-0442(2001)014<0255:AATOSI>2.0.CO;2.

Wang, J., J. Zhang, E. Watanabe, M. Ikeda, K. Mizobata, J. E. Walsh, X. Bai, and B. Wu, 2009: Is the dipole anomaly a major driver to record lows in arctic summer sea ice extent? *Geophys. Res. Lett.,* **36,** L05706, doi:10.1029/2008GL036706.

Watanabe, E., and H. Hasumi, 2005: Arctic sea ice response to wind stress variations. *J. Geophys. Res.,* **110,** C11007, doi:10.1029/2004JC002678.

Wu, B., J. Wang, and J. E. Walsh, 2006: Dipole anomaly in the winter Arctic atmosphere and its association with sea ice motion. *J. Climate,* **19,** 210–225, doi:10.1175/JCLI3619.1.

Zhang, J., R. Woodgate, and R. Moritz, 2010: Sea ice response to atmospheric and oceanic forcing in the Bering Sea. *J. Phys. Oceanogr.,* **40,** 1729–1747, doi:10.1175/2010JPO4323.1.

Zhang, X., M. Ikeda, and J. E. Walsh, 2003: Arctic sea ice and freshwater changes driven by the atmospheric leading mode in a coupled sea ice–ocean model. *J. Climate,* **16,** 2159–2177, doi:10.1175/2758.1.

Zubov, N. N., 1943: *Arctic Ice.* U.S. Navy Electronics Laboratory, 506 pp.